Suppression of the type Ia supernova host galaxy step in the outer regions of galaxies

M. Toy,[1] P. Wiseman,[1] M. Sullivan,[1] D. Scolnic,[2] M. Vincenzi,[2,3,4] D. Brout,[5] T. M. Davis,[6]
C. Frohmaier,[1] L. Galbany,[7,8] C. Lidman,[9,10] J. Lee,[11] L. Kelsey,[12] R. Kessler,[13,14] A. Möller,[15] B. Popovic,[2]
B. O. Sánchez,[2,16] P. Shah,[17] M. Smith,[18] S. Allam,[19] M. Aguena,[20] O. Alves,[21] D. Bacon,[12] D. Brooks,[17]
D. L. Burke,[22,23] A. Carnero Rosell,[24,20] J. Carretero,[25] L. N. da Costa,[20] M. E. S. Pereira,[26] S. Desai,[27]
H. T. Diehl,[19] P. Doel,[17] A. Drlica-Wagner,[13,19,14] S. Everett,[28] I. Ferrero,[29] B. Flaugher,[19] J. Frieman,[19,14]
J. García-Bellido,[30] M. Gatti,[11] E. Gaztanaga,[7,12,8] G. Giannini,[25,14] R. A. Gruendl,[31,32] G. Gutierrez,[19]
S. R. Hinton,[6] D. L. Hollowood,[33] K. Honscheid,[34,35] D. J. James,[5] O. Lahav,[17] S. Lee,[36] J. L. Marshall,[37] J.
Mena-Fernández,[38] R. Miquel,[39,25] A. Palmese,[40] A. Pieres,[20,41] A. A. Plazas Malagón,[22,23] A. K. Romer,[42]
S. Samuroff,[43] E. Sanchez,[44] D. Sanchez Cid,[44] M. Schubnell,[21] E. Suchyta,[45] M. E. C. Swanson,[31]
G. Tarle,[21] D. L. Tucker,[19] V. Vikram,[46] A. R. Walker,[47] and N. Weaverdyck[48,49]

(DES Collaboration; Affiliations can be found at after the References.)

ABSTRACT

Using 1533 type Ia supernovae (SNe Ia) from the five-year sample of the Dark Energy Survey (DES), we investigate the effects of projected galactocentric separation between the SNe and their host galaxies on their light curves and standardization. We show, for the first time, that the difference in SN Ia post-standardization brightnesses between high and low-mass hosts reduces from 0.078 ± 0.011 mag in the full sample to 0.036 ± 0.018 mag for SNe Ia located in the outer regions of their host galaxies, while increasing to 0.100 ± 0.014 mag for SNe in the inner regions. In these inner regions, the step can be reduced (but not removed) using a model where the R_V of dust along the line-of-sight to the SN changes as a function of galaxy properties. To explain the remaining difference, we use the distributions of the SN Ia stretch parameter to test whether the inferred age of SN progenitors are more varied in the inner regions of galaxies. We find that the proportion of high-stretch SNe Ia in red (older) environments is more prominent in outer regions and that the outer regions stretch distributions are overall more homogeneous compared to inner regions, but conclude that this effect cannot explain the reduction in significance of any Hubble residual step in outer regions. We conclude that the standardized distances of SNe Ia located in the outer regions of galaxies are less affected by their global host galaxy properties than those in the inner regions.

Key words: transients: supernovae – supernovae: general – cosmology: observations – distance scale

1 INTRODUCTION

Type Ia supernovae (SNe Ia) are a mature cosmological probe. The industrialisation of their discovery, measurement and analysis provides a 'standardizable candle' giving unparalleled insight into the Universe's expansion history, particularly in the redshift $z < 0.6$ Universe where dark energy dominates. However, despite the established consensus of an exploding carbon-oxygen white dwarf star with a light curve powered by the radioactive decay of ^{56}Ni, there remain open questions over the details of the configuration of the progenitor systems, their explosion physics, and the effect of dust on their light curves and luminosities.

It is well known that SN Ia photometric properties have dependencies on the environment in which the SNe explode. For example, intrinsically brighter and slower evolving SNe Ia tend to explode in younger stellar populations (Hamuy et al. 2000). For cosmological applications, such large scale environmental effects can be removed after the application of standardization relations between SN Ia luminosity and SN light-curve width (Phillips 1993), and SN Ia luminosity and SN optical colour (Riess et al. 1996; Tripp 1998).

More concerning for cosmological measurements is the observation that, even after such standardization, the brightnesses of SNe Ia (and thus the distances inferred to them) have a residual dependence on the properties of the galaxy in which they exploded. SNe Ia in massive, passive, older galaxies are brighter post standardization, and those in low-mass, younger, star-forming galaxies are fainter. Simplistically, this manifests as a step in SN Ia post-standardization luminosity at a host galaxy stellar mass close to 10^{10} $M_\odot$ (Kelly et al. 2010; Sullivan et al. 2010; Lampeitl et al. 2010). This so-called 'mass step' is observed or routinely modelled in all large SN Ia sur-

veys or compilations of datasets (e.g., Betoule et al. 2014; Brout et al. 2022; DES Collaboration et al. 2024; Ginolin et al. 2024a) and has a typical size of about 0.06–0.15 mag (or three to seven per cent in distance) depending on the details of the sample. Similar trends are seen when replacing host stellar mass with other global host galaxy properties such as star-formation rate (SFR; Rigault et al. 2013), rest-frame colours (Roman et al. 2018; Jones et al. 2018b) or gas-phase/stellar metallicity (Childress et al. 2013; Moreno-Raya et al. 2016; Millán-Irigoyen et al. 2022), and when considering these properties measured locally in a small aperture at the SN position (Rigault et al. 2013; Roman et al. 2018; Kelsey et al. 2021).

The origin of the mass step is controversial and has implications that extend beyond SN Ia cosmology. Explanations include changing properties of the progenitor star, e.g., age (Rose et al. 2019; Rigault et al. 2020) or metallicity (Hayden et al. 2013), differing progenitor systems themselves, or dust properties that change with galaxy stellar mass (Brout & Scolnic 2021, hereafter BS21). This latter explanation, where the ratio of total-to-selective extinction R_V is different in low and high-mass galaxies, also provides an explanation for the variation of the step size with SN colour, with redder SNe appearing to show a larger step (Brout & Scolnic 2021). At the time of writing, no single astrophysical origin for the mass step appears to explain all of the SN Ia observations (Thorp & Mandel 2022; Wiseman et al. 2023; Popovic et al. 2024a).

In this paper, we explore whether the position of a SN Ia in its host galaxy can provide additional information on the mass step puzzle, in particular the projected separation of a SN from its host galaxy (or galactocentric distance). There are strong astrophysical motivations for examining this in more detail: it has long been known that galaxies often show radial gradients in metallicity, age and dust content (e.g., Searle 1971; Pagel & Edmunds 1981; Kormendy & Djorgovski 1989; Maiolino & Mannucci 2019; Parikh et al. 2021). These may act as a proxy for the SN Ia progenitor star and its environment. For example, stellar populations in late-type galaxies are typically younger in the outer regions with a lower scatter in the ages measured (Goddard et al. 2017; Parikh et al. 2021), whereas stellar populations in early-type galaxies may be older in the outer regions (Baes et al. 2007; Goddard et al. 2017) or exhibit little overall gradient. Similarly, both star-forming (Simpson et al. 1995; Sánchez et al. 2014) and early-type galaxies (Kormendy & Djorgovski 1989) show negative gradients in their metal abundances (González Delgado et al. 2014, 2015), with inner galactic regions being more metal rich than the outer regions.

Work using various samples of SNe Ia of order 100 events showed no clear trends between SN Ia light-curve width and their projected galactocentric distance (Ivanov et al. 2000; Jha et al. 2007; Hicken et al. 2009; Yasuda & Fukugita 2010). Using a larger sample of ∼ 1000 events from the Dark Energy Survey five-year sample, Toy et al. (2023) showed a deficit of brighter and more slowly evolving (high 'stretch') SNe Ia in the centres of galaxies. This is unlikely to originate from an observational bias: the well-known increased difficulty of finding SNe Ia in galactic centres due to the increased surface brightness would not bias towards detecting the faster, fainter SNe that appear preferentially hosted in these regions.

In terms of SN Ia colour (or extinction), there is some evidence that extincted (red) SNe Ia are not found at large galactocentric distances (Jha et al. 2007; Hicken et al. 2009) and are instead found more centrally in spiral or star-forming galaxies (Galbany et al. 2012; Anderson et al. 2015). Using 302 SNe Ia from the SDSS SN survey (Sako et al. 2018), Hill et al. (2018) showed a statistically significant difference in the observed SN Ia colour distributions between events that are nearer (redder SNe) and further (bluer SNe) from their host galaxy centres, confirmed in the recent release of ~1000 low-

redshift SNe Ia from the Zwicky Transient Facility (ZTF; Ginolin et al. 2024b).

Studies into the cosmological effects of galactocentric distances on SN Ia distance determination have been limited. No clear results were found in the low-redshift sample of Hicken et al. (2009). However, Hill et al. (2018) and Uddin et al. (2020) report a smaller residual scatter in SN Ia Hubble residuals at larger galactocentric distances. There is also some evidence that galactic position may influence other SN Ia properties. 'High velocity' SNe Ia, defined as those SNe Ia with silicon velocities measured from their spectra in excess of 12,000 km s^{-1}, are found preferentially in the centres of their host galaxies (Wang et al. 2013; Pan et al. 2015; Nugent et al. 2023).

We use the Dark Energy Survey (DES) SN programme five-year dataset (Sánchez et al. 2024) to examine the effect of galactocentric distance on SN Ia standardization. The DES-SN5YR dataset is a well-calibrated and understood high-redshift SN Ia cosmological dataset, with deep imaging data available for the SN Ia host galaxies (Wiseman et al. 2020). Throughout, where relevant we assume a reference cosmology of a flat ΛCDM universe with $\Omega_{matter} = 0.3$, and with a Hubble constant of $H_0 = 70$ km s^{-1} Mpc^{-1}.

2 DATA

In this section we introduce the dataset that we use in this paper: the 'five-year' SN Ia sample (Möller et al. 2022; Sánchez et al. 2024) from the DES SN programme (DES-SN5YR). We use 1533 SNe Ia from the 'cosmological sample' of Vincenzi et al. (2024) selected from all DES-SN5YR SNe Ia based on the quality of the SN light curves and their light-curve fits (see their table 4). All events are photometrically-identified as SNe Ia (Möller & de Boissière 2020) with $P_{Ia} > 0.5$, where P_{Ia} is the probability of the event being a SN Ia. All the SNe Ia have a spectroscopic redshift of their host galaxy typically from the follow-up OzDES survey (Lidman et al. 2020). This number differs from the 1541 reported in Vincenzi et al. (2024) due to an extra requirement in the bias correction stage (Section 2.1).

The host galaxies themselves were identified from a catalogue generated from deep, stacked $griz$ images from DES free of SN light (Wiseman et al. 2020), using the Source Extractor software (Bertin & Arnouts 1996) to measure host positions, structural parameters and photometry. SNe were matched to candidate host galaxies using the directional light radius (DLR) method (Sullivan et al. 2006; Gupta et al. 2016; Sako et al. 2018). The host galaxy photometry has been fit with a series of galaxy spectral energy distribution (SED) templates to estimate host stellar masses (M_*), SFRs and $U - R$ rest-frame colours following Sullivan et al. (2006) and Kelsey et al. (2021) as implemented in DES-SN5YR (Smith et al. 2020). Galaxy rest-frame colours are reported in Bessell (1990) passbands and in the Vega magnitude system (Johnson & Morgan 1953). These rest-frame colours are calculated using the method outlined in Kelsey et al. (2021), where the best-fitting host galaxy SED for each SN is adjusted with a wavelength-dependent multiplicative function such that the SED exactly reproduces the observed DES $griz$ photometry (often referred to as 'mangling' Hsiao et al. 2007; Conley et al. 2008).

2.1 SN Ia distances and bias corrections

The SN Ia light curves have been fit with the SALT3 light-curve model (Guy et al. 2007; Kenworthy et al. 2021; Taylor et al. 2023) to estimate various light curve parameters. Of particular relevance are x_1, a 'stretch'-like parameter (Perlmutter et al. 1997) that measures the width of each SN light curve relative to a template, and c, a
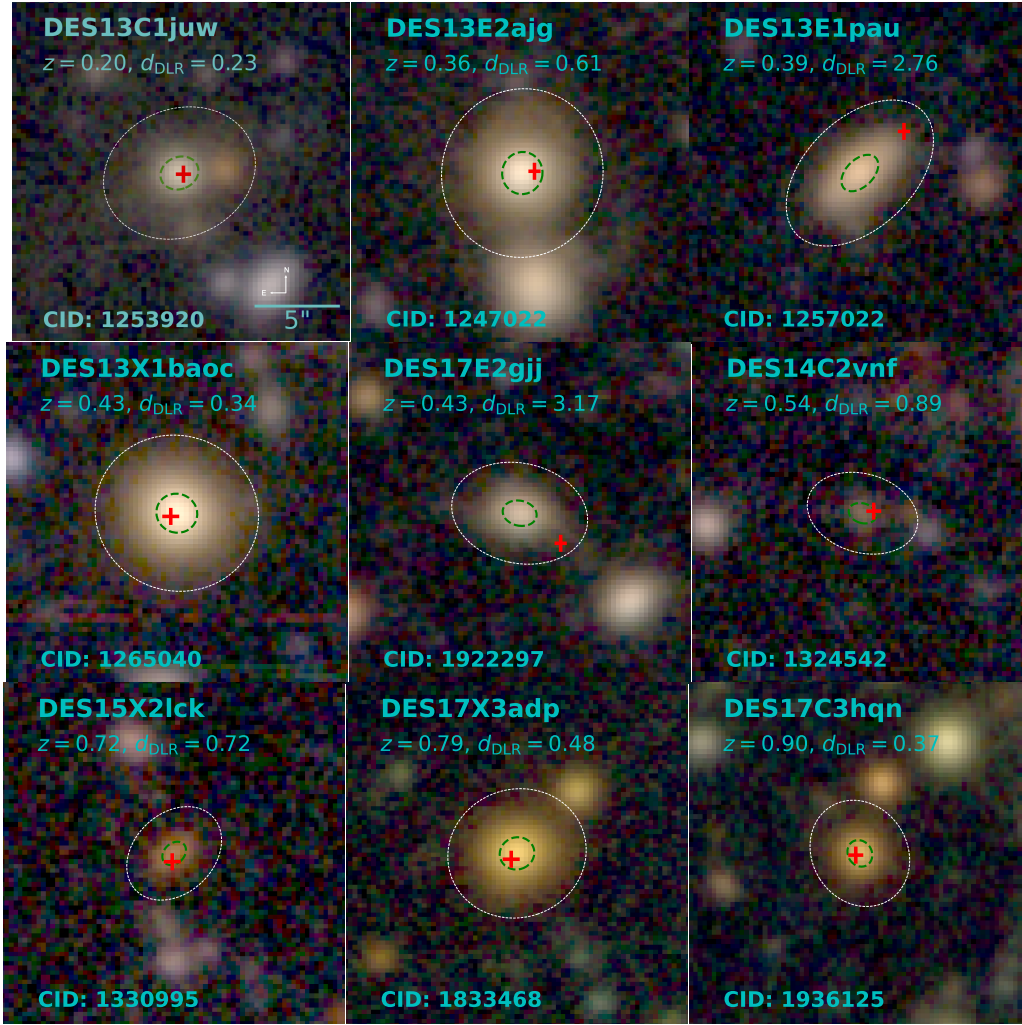
Figure 1. Montage of a selection of DES SN Ia host galaxies with the SN position marked as a red cross, together with the elliptical apertures defined by $d_{\mathrm{DLR}} = 1$ (green) and $d_{\mathrm{DLR}} = 4$ (white). Both the DES SN name and the DES search pipeline candidate ID (CID) are shown. Each image is 20 arcseconds on each side.

colour parameter that is similar to the rest-frame $B - V$ colour of a SN. Distances to the SNe, μ_{obs}, are then estimated using (e.g., Tripp 1998; Astier et al. 2006)

$$\mu_{\mathrm{obs}} = m_x + \alpha x_1 - \beta c - \mathrm{M} - \mu_{\mathrm{bias}}, \qquad (1)$$

where m_x, x_1 and c are the SALT3 SN light-curve parameters, α and β are global nuisance parameters parametrizing the stretch–luminosity and colour–luminosity relations, and M is the absolute magnitude of a SN Ia with $x_1 = 0$ and $c = 0$. μ_{bias} is the bias term that corrects for various observational and astrophysical selection effects.

Hubble residuals $\Delta\mu$ are then defined as

$$\Delta\mu = \mu_{\mathrm{obs}} - \mu_{\mathrm{model}}, \qquad (2)$$

where μ_{obs} is defined in equation 1 and μ_{model} is the distance modulus in a reference cosmology. The Hubble residuals indicate whether a given SN Ia is brighter or fainter than expected in the reference cosmology; negative residuals indicate a brighter event.

In our analysis we differ from the main DES-SN5YR analysis in three ways. Firstly, we do not include a 'γG_{host}' term in equation 1. When used, such a term is designed to encapsulate any residual dependencies between SN Ia luminosities and their host galaxy properties (such as a stellar mass step) that are not corrected for in the

light-curve fitting or bias correction steps. As a goal of our paper is to investigate such host galaxy effects, we do not apply this correction.

The second difference is in our use of bias corrections (μ_{bias}). The bias corrections account for selection biases in the DES SN Ia sample, for example as a function of redshift, SN light curve parameters, or host galaxy properties. The corrections are generally estimated using a Monte Carlo approach modelling the survey detection efficiency and other potential selection effects given assumptions about the underlying SN Ia populations (Kessler et al. 2009; Perrett et al. 2010; Betoule et al. 2014). Early use of simulations modelled distance bias corrections as a function of redshift only (Kessler et al. 2009; Jones et al. 2018a) but other approaches have included effects due to stretch and colour (Scolnic & Kessler 2016) and incorporated models relating SN properties and their host galaxies (Popovic et al. 2023).

The DES-SN5YR analysis uses the approach of Popovic et al. (2021), with bias corrections modelled as a function of z, x_1, c, and $\log(M_*)$ using the 'Beams with Bias Corrections' method (BBC; Kessler & Scolnic 2017). We refer to this approach as 'BBC 4D' (see discussion in Vincenzi et al. 2024). This framework includes an underlying model that makes assumptions about how SNe Ia and dust vary by host properties, which is part of the motivation for this paper. Therefore, we use as our main analysis a simpler

'1D' approach, which implements bias corrections only as a function of redshift, accounting for Malmquist-like biases (Malmquist 1922, 1925) but making no reference to host galaxies in the bias corrections. However, we also include a comparison with the BBC 4D results where relevant. In the BBC framework, SNe that do not achieve a valid bias correction are removed from the analysis. Throughout this work we use the sample of SNe that pass both the 1D and the 4D bias corrections, leaving us with 1533 SNe.

The third difference is that the main DES-SN5YR analysis uses a low-z sample in order to anchor the Hubble diagram, which is important when measuring cosmological parameters. Here, we investigate only the DES-SN5YR SNe Ia and do not include a low-z sample (and hence, we use a reference cosmology for all Hubble residual calculations).

In estimating our distances using BBC 1D, we recover nuisance parameter values of $\alpha = 0.159 \pm 0.009$ and $\beta = 2.73 \pm 0.05$. These differ from those reported in table 5 of Vincenzi et al. (2024), as those values were estimated using the BBC 4D bias corrections, but are similar to other estimates of α and β found for the DES-SN5YR sample using 1D corrections (e.g., Kelsey et al. 2023).

2.2 SN–host separations

SN celestial coordinates (x_{SN}, y_{SN}) were measured by DES using point-spread function (PSF) fitting photometry (Kessler et al. 2015), with the coordinates computed using the weighted-average from each measurement during an observing 'season'. Host galaxies were detected and measured in the DES image stacks by (Wiseman et al. 2020) using Source Extractor. We use the celestial coordinates (image centroids) of the Source Extractor detections (x_{host}, y_{host}) measured from images with the same world coordinate system as the images on which x_{SN}, y_{SN} are determined. These then define the angular separation (or projected galactocentric distance), $\Delta\theta$, between the SN and the centre of the host galaxy, i.e.,

$$\Delta\theta = \sqrt{(x_{SN} - x_{host})^2 + (y_{SN} - y_{host})^2}. \tag{3}$$

The DES host galaxies cover a broad range of sizes, stellar masses, inclinations and redshifts; even if converted to physical units (e.g., kpc), the galactocentric distances are not fairly comparable between events if the apparent size of the host galaxy itself varies. Normalising the galactocentric distances using an effective radius or scale length does help, but does not account for inclination effects. We therefore use the DLR as our normalisation of the galactocentric distances, which accounts for the apparent size of a host galaxy in the direction of a SN.

To measure DLRs, we use the Source Extractor basic shape parameters A (semi-major axis) and B (semi-minor axis) that define the elliptical shape of the detected galaxy. The scales of A and B are set by the second-order moments (variance) of the galaxy's profile along the A and B axes (e.g., Stobie 1980).

The DLR is then defined as[1]

$$DLR = \frac{AB}{\sqrt{(A\sin\phi)^2 + (B\cos\phi)^2}}, \tag{4}$$

where ϕ is the angle between the semi-major axis and the vector of interest, in our case a vector connecting the centre of the galaxy to the SN position. The DLR host-matching algorithm chooses the galaxy with the smallest d_{DLR}, which is defined as the ratio between

---

[1] The definition in Sullivan et al. (2006) is in terms of Source Extractor CXX, CYY, and CXY ellipse parameters, but is mathematically equivalent.

$\Delta\theta$ and the DLR in the direction of the SN. In other words, d_{DLR} measurements are SN–host separations normalised to the size of the host galaxy being compared in the direction to the SN. An upper limit of $d_{DLR} = 4$ is used; Qu et al. (2024) show that < 2 per cent of our SNe are likely to be associated with the wrong host galaxy. We show a montage of representative host galaxies and their SN positions in Fig. 1, with the $d_{DLR} = 1$ and $d_{DLR} = 4$ elliptical apertures overplotted. The d_{DLR} values for all DES-SN5YR SNe Ia can be found in the Sánchez et al. (2024) data release.

The distribution of d_{DLR} in our sample is shown in Fig. 2, together with the variation of d_{DLR} with redshift (see also Qu et al. 2024). We see no redshift-dependent trends.

Seeing effects are important in our host galaxy sample: the number of resolution elements for each of our host galaxies is small given the typical image quality (PSF FWHM) in our image stacks of $\simeq 1.3''$ (Kelsey et al. 2021). A useful characteristic of d_{DLR} is that it is purely empirical and reproducible. There is no model dependency, i.e., fitting a Sérsic (1963) profile or sophisticated bulge/disc decomposition is not required. This is important in our high-redshift sample where we have very little (if any) morphological information and complicated model fits can become unconstrained.

A useful rule of thumb for physically interpreting DLR is that, for a galaxy with a 2D Gaussian profile, the elliptical shape defining the galaxy detection of radius DLR (on average around 6 kpc for our sample) for any ϕ will contain $\simeq 68$ per cent of the galaxy light. A DLR of three for any ϕ typically represents the isophotal limit of a galaxy's detection in that direction, and the commonly-used galaxy effective radius (or half light radius) is $\simeq 0.67$ DLR.

3 SN IA PROPERTIES AS A FUNCTION OF GALACTOCENTRIC DISTANCE

In this section we examine how SN Ia properties depend on their galactocentric distance. We begin with the simple photometric properties of light-curve width and colour, and then investigate their Hubble residuals.

3.1 Light curve properties

The SALT3 SN x_1 and c distributions as a function of d_{DLR} are shown in Fig. 3. We give the mean values of the SALT3 x_1 and c parameters for both inner and outer regions, using different d_{DLR} values to define these, in Table 1. As expected, on average SNe Ia located within the innermost regions ($d_{DLR} \leq 0.5$) of the host galaxy have a smaller x_1 than those located at $d_{DLR} > 0.5$ (Toy et al. 2023). This means that, on average, SNe within the centres of galaxies are faster evolving than SNe at higher galactic radii. This not surprising: these are likely to be the oldest stellar populations in galaxies, and there are known correlations between light-curve shape and stellar population age (e.g., Hamuy et al. 2000).

In SN colour there are no strong trends, but SNe Ia at $d_{DLR} \leq 1$ are slightly redder (higher c) than those at $d_{DLR} > 1$, and at $d_{DLR} > 1.5$ the SNe appear bluer on average than those closer to the galaxy centres with a smaller scatter in c. There are no red SNe Ia ($c > 0.2$) at high d_{DLR}, consistent with the earlier results of Hill et al. (2018) and Ginolin et al. (2024b). As redder and faster SNe Ia are fainter, it is difficult to imagine a selection effect that would bias in favour of these events in the bright inner regions of galaxies.
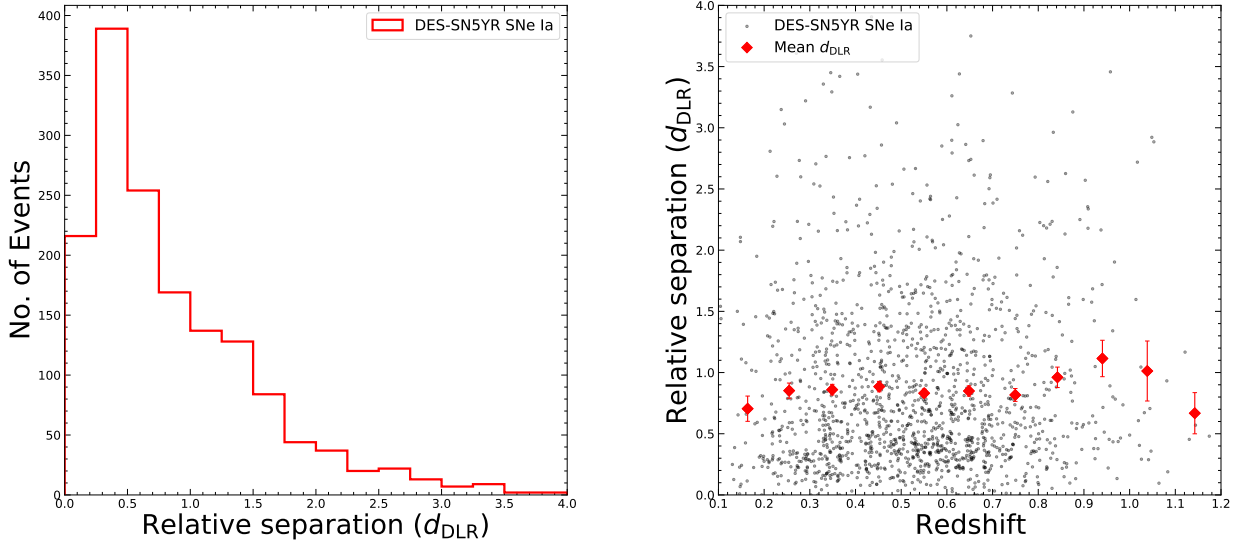
Figure 2. The distribution of d_{DLR} in our sample (left) together with its variation with redshift (right). On the right, the red points show the mean d_{DLR} and uncertainty in bins of redshift.
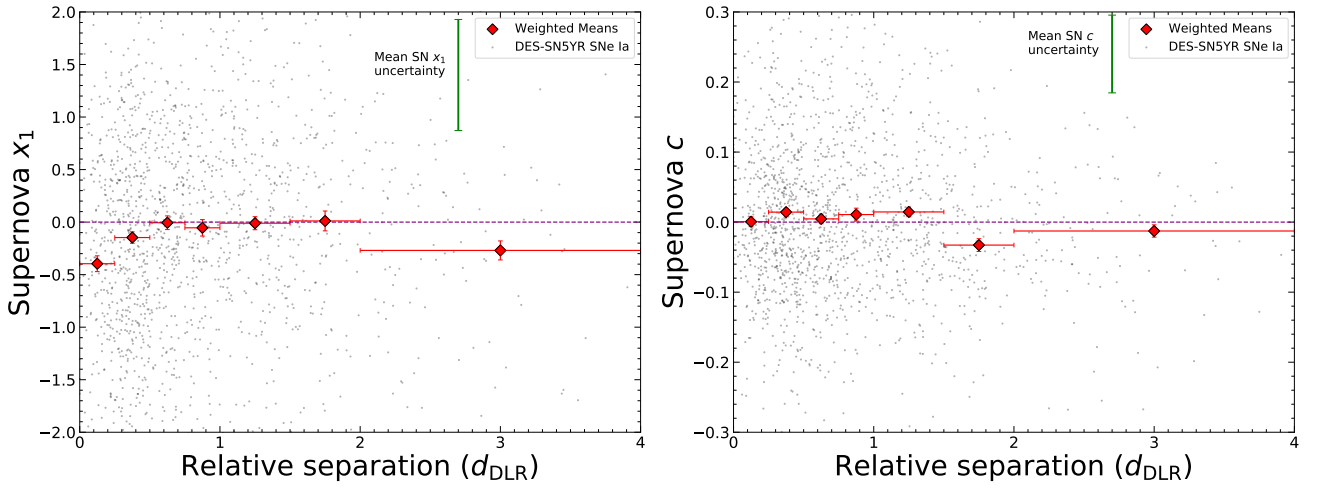

Figure 3. SALT3 SN Ia x_1 (left) and SN Ia colour c (right) for our sample as a function of d_{DLR}. The black points are our full sample, and the red points show weighted mean values in bins of d_{DLR}. The typical uncertainty in x_1 and c are shown as the green error bars. No bias corrections have been applied to the x_1 and c values. Note the decrease in mean x_1 in the centres of host galaxies.

Table 1. Weighted mean values of SN Ia light curve properties x_1 and c and Hubble residuals in different d_{DLR} ranges.

d_{DLR} range	Number of SNe Ia	$\bar{x}_1$	$\bar{c}$	Mean $\Delta\mu$
$d_{DLR} \leq 0.5$	607	-0.24 ± 0.04	0.009 ± 0.004	-0.012 ± 0.010
$d_{DLR} > 0.5$	926	-0.05 ± 0.03	0.001 ± 0.003	0.008 ± 0.007
$d_{DLR} \leq 1.0$	1028	-0.16 ± 0.03	0.008 ± 0.003	0.001 ± 0.007
$d_{DLR} > 1.0$	505	-0.07 ± 0.05	-0.002 ± 0.005	-0.002 ± 0.009
$d_{DLR} \leq 1.5$	1294	-0.12 ± 0.03	0.010 ± 0.003	0.002 ± 0.006
$d_{DLR} > 1.5$	239	-0.14 ± 0.07	-0.023 ± 0.006	-0.009 ± 0.014
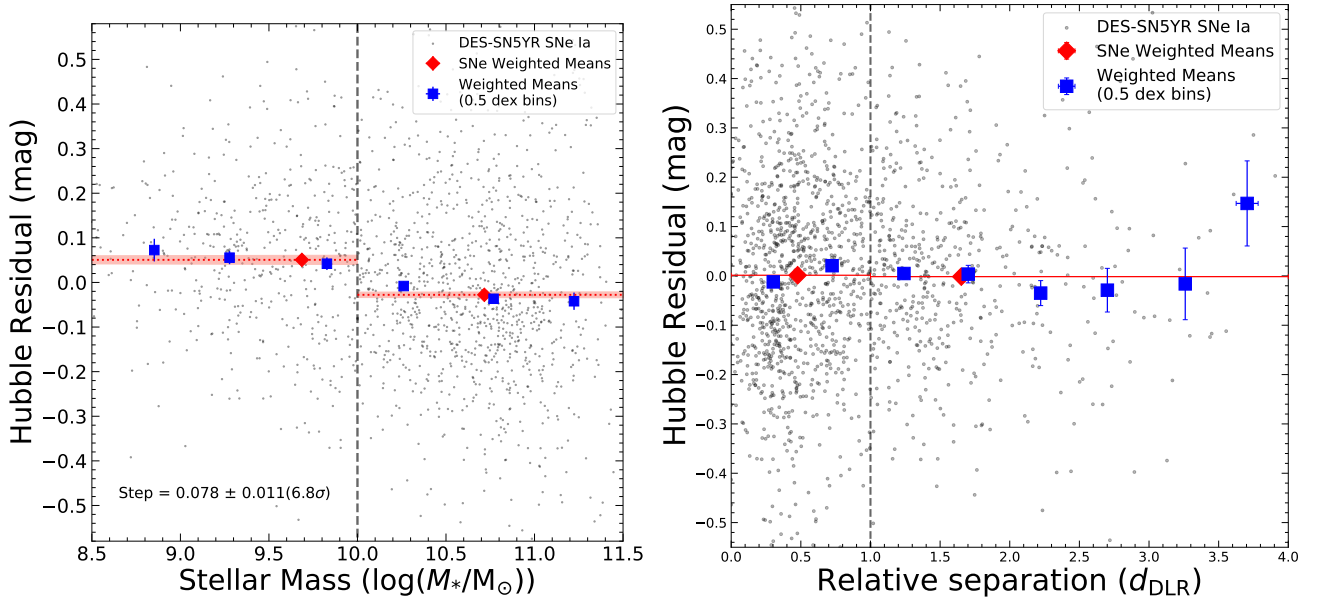
Figure 4. Hubble residuals (equation 2) for the DES-SN5YR photometric sample, with 1D bias corrections (Section 2.1), as a function of their host galaxy stellar mass (left) and galactocentric distance d_{DLR} (right). In both panels, the blue points show the mean residuals in bins of 0.5 dex, while the red points and shaded areas show the mean residuals and their uncertainty for SNe Ia to the left and right of the vertical dashed lines. For stellar mass, when divided into bins above and below a stellar mass of 10^{10} M$_\odot$, there is a difference in Hubble residuals of 0.072 ± 0.012 mag; the so-called 'mass step'. For d_{DLR}, there is no difference in Hubble residual when splitting the sample at $d_{DLR} = 1$ (0.0028 ± 0.012 mag). However, when restricting the sample to $d_{DLR} \leq 1$, and splitting at $d_{DLR} = 0.5$, there is a small step of 0.033 ± 0.011 mag.

3.2 Hubble residuals

We next examine the SN Ia Hubble residuals, shown versus host galaxy stellar mass in Fig. 4. We remind the reader that we are using Hubble residuals corrected using 1D bias corrections (i.e., correcting for redshift biases only) as opposed to the nominal values presented in Vincenzi et al. (2024) that use the BBC 4D method. This is because we are aiming to understand the causes of Hubble residual–host galaxy correlations, which the 4D approach attempts to model.

As expected based on previous studies of the DES data (e.g., Kelsey et al. 2023), the SN Ia luminosity step in host galaxy stellar mass ('mass step') is clearly seen in the DES-SN5YR sample with a size of 0.072 ± 0.012 mag ($\sim 6\,\sigma$). The size of this step is consistent with earlier studies.

3.2.1 Hubble residuals as a function of d_{DLR}

In the right hand panel of Fig. 4 we show the variation in Hubble residual with d_{DLR}. While previous studies with smaller samples have generally shown null results in similar tests (e.g., Hicken et al. 2009; Galbany et al. 2012), here we see a mild trend: when splitting the sample at $d_{DLR} = 0.5$, SNe Ia have more negative Hubble residuals in the inner regions of galaxies. The step is small: 0.020 ± 0.012 mag (Table 1), which increases to 0.033 ± 0.011 mag when only considering events within $d_{DLR} \leq 1$. However, if we split at $d_{DLR} = 1$, we find no difference between the mean Hubble residuals.

The trend itself is not unexpected given the known relationships between Hubble residual and stellar mass (e.g., left panel of Fig. 4): regions within $d_{DLR} < 0.5$ are likely to be similar to the old, passive stellar environments of massive galaxies, and the outer regions similar to those in younger lower mass galaxies. A logical next step is to test how the Hubble residual–d_{DLR} trend relates to the well-known stellar mass and host galaxy colour steps.

3.2.2 Host stellar mass step and d_{DLR}

We show the host galaxy stellar mass step separately for SNe Ia in bins of d_{DLR} and find that the size of the stellar mass step does depend on the galactocentric distance (Fig. 5). Step sizes and their significance are reported in Table 2. The greatest disparity occurs at $d_{DLR} = 1$: within that radius, SNe have a mass step of 0.100 ± 0.014 mag ($6.9\,\sigma$), whereas for $d_{DLR} > 1$ the step is consistent with zero (0.036 ± 0.018 mag; $2.0\,\sigma$). Recall that we have made no attempt in our bias correction methodology to model the host mass step: the step is simply not present in our sample with $d_{DLR} > 1$.

We additionally calculate the root-mean-square deviation (r.m.s), σ_{rms}, in the Hubble residuals for SNe Ia in host galaxies on either side of the mass step. The σ_{rms} for outer region SNe Ia is 0.02–0.03 mag smaller in both lower and higher mass host galaxies than for SNe Ia in the inner regions (Table 2). This modest reduction may indicate a more robust standardization for SNe in the outer regions compared to the inner regions, consistent with results in the literature (e.g., Hill et al. 2018; Uddin et al. 2020).

We verify the robustness of the change in mass step sizes at $d_{DLR} \leq 1$ and $d_{DLR} > 1$ by bootstrap resampling. We select (with replacement) the same number of SNe as in the outer regions (505) randomly from the full sample of 1533 events. We weight this selection so that the resampled SNe have the same colour distribution as those truly in the outer regions. We then calculate the size and significance of any host mass step in each resample. The results for 10^5 draws (resamples) are shown in Fig. 6. On average, the step size in resamples is consistent with the full sample, although less significant given the smaller sample size ($\bar{\sigma} = 4.7 \pm 0.75$ versus $\sigma \simeq 6$). We conclude that the reduced mass step in SNe Ia located in the outer regions is unlikely to be due to random chance.

To determine if the observed difference in mass step size between inner and outer regions is best fit by a single step at $d_{DLR} = 1$, we
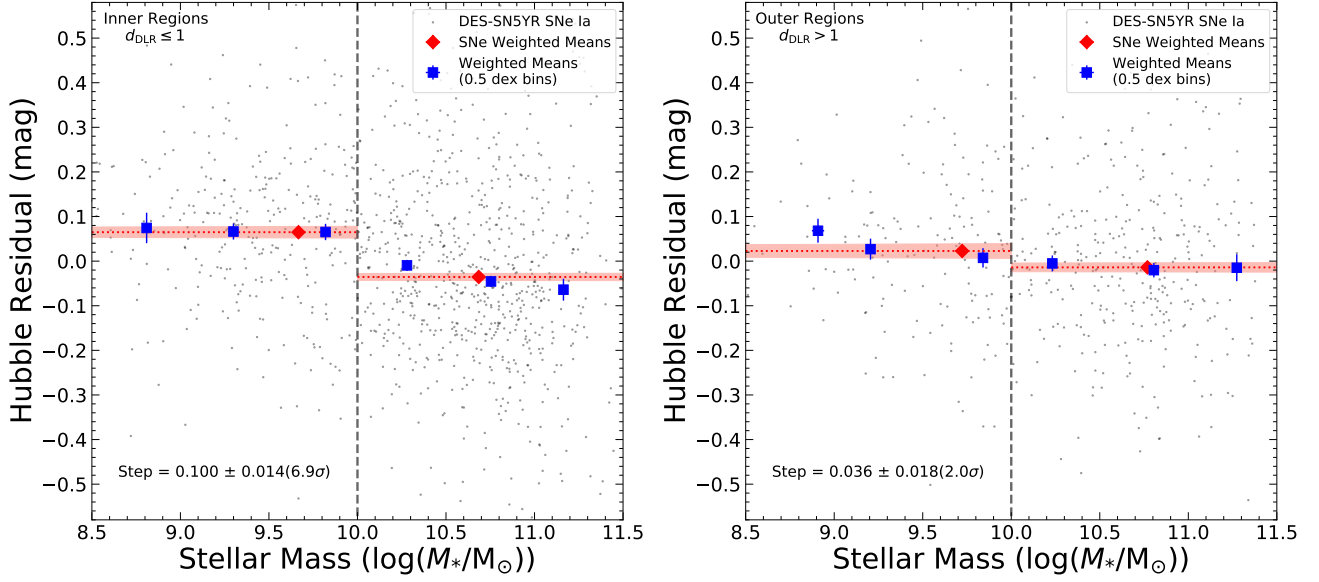
Figure 5. The SN Ia mass step (Fig. 4, left), but limited to SNe Ia with $d_{DLR} \leq 1$ (left) and $d_{DLR} > 1$ (right). The mass step sizes are 0.100 ± 0.014 mag (left) and 0.036 ± 0.018 mag (right), i.e., the size of the mass step is reduced when restricting to SNe Ia located in the outer regions of their host galaxies.

Table 2. Statistics related to the steps in SN Ia luminosity as a function of stellar mass (the mass step) in our samples.

Sample	Number (LM hosts, HM hosts)	Mean $\Delta\mu$ in low-mass hosts	Mean $\Delta\mu$ in high-mass hosts	Size of the mass step	Significance of step	r.m.s in low-mass hosts	r.m.s in high-mass hosts
Full Sample	1533 (472, 1061)	0.051 ± 0.009	-0.028 ± 0.007	0.078 ± 0.011	6.8σ	0.199	0.226
$d_{DLR} \leq 1$	1028 (310, 718)	0.065 ± 0.012	-0.035 ± 0.009	0.100 ± 0.014	6.9σ	0.205	0.232
$d_{DLR} > 1$	505 (162, 343)	0.023 ± 0.014	-0.014 ± 0.011	0.036 ± 0.018	2.0σ	0.180	0.212
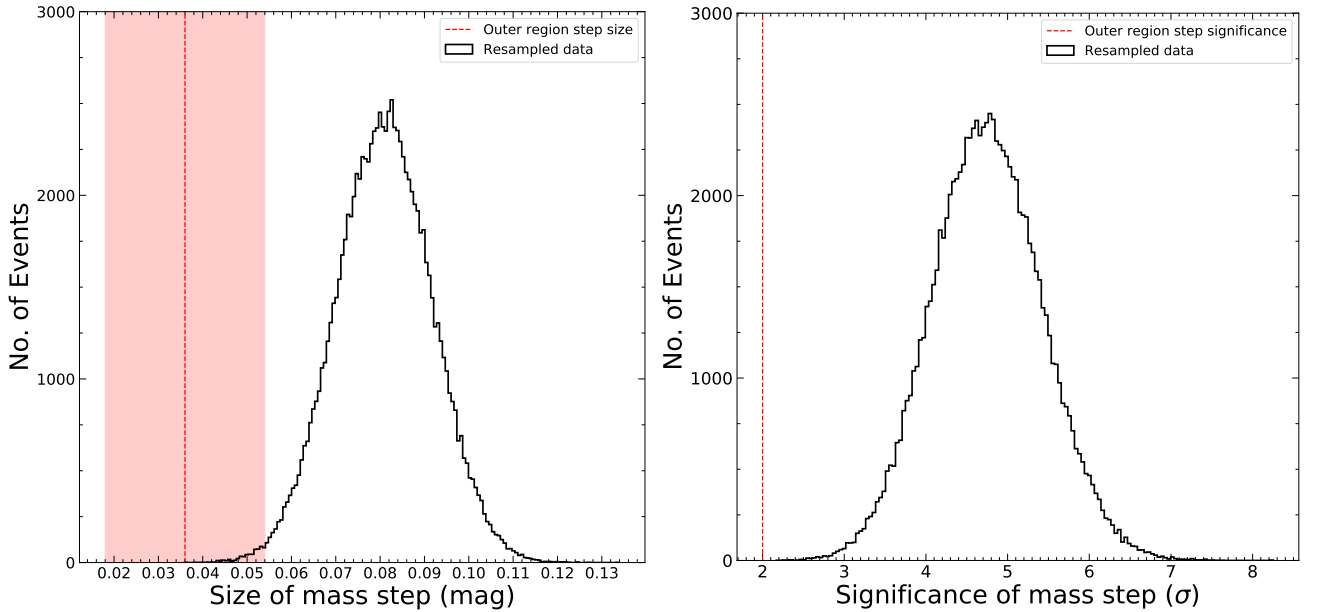
Figure 6. Bootstrap resampling test of the significance of the reduction of the mass step observed in SNe Ia in the outer regions of their host galaxies ($d_{DLR} \leq 1$). SNe are selected with replacement from the full sample to match the size and colour distribution of the true sample of SNe Ia in the outer regions. We perform 10^5 such resamples and show histograms of the results. Left: The distribution of host mass step size in the 10^5 resamples. The distribution of the mass step in the resampled SNe is centred on a step size of 0.08 mag, consistent with the host mass step observed in our full sample. Right: The distribution of host mass step significance. On average, a statistically significant step is found for our resampled SNe. The dashed vertical lines show the actual values measured in the real data for SNe in the outer regions.

use smaller d_{DLR} bins, each with a similar number of SNe Ia. We also fit a straight line to the data. The results are shown in Fig. 7. The figure shows a clear difference in step size between $d_{\mathrm{DLR}} \leq 1$ and $d_{\mathrm{DLR}} > 1$, i.e., the result in Fig. 5 is not dependent on the choice of $d_{\mathrm{DLR}} = 1$ to divide the sample.

3.2.3 Host colour steps and d_{DLR}

Complementary to stellar mass, host galaxy colour also correlates strongly with Hubble residual with at least equal (if not greater) significance than stellar mass (Roman et al. 2018; Kelsey et al. 2023; Briday et al. 2022; Wiseman et al. 2022, 2023). Galaxy colours trace a combination of the age of the stellar population and to a lesser extent the integrated dust extinction, and the correlations between Hubble residual and galaxy colour are often interpreted as the age of the SN progenitor system (or a combination of the progenitor and its surrounding environment such as dust along the line of sight) as being the driver of the step.

We show the host galaxy rest-frame $U - R$ colour versus Hubble residuals in Fig. 8. We split the SN Ia sample at host $U - R = 1$ following Kelsey et al. (2021, 2023). The step sizes are similar to those for stellar mass: SNe Ia within $d_{\mathrm{DLR}} \leq 1$ have a strong Hubble residual step between red and blue hosts, while the step between SNe in red and blue hosts at $d_{\mathrm{DLR}} > 1$ is reduced to $\sim 2\,\sigma$.

The global galaxy colour traces the galaxy-integrated properties. To understand better whether the observed d_{DLR} effects are driven by stellar population age, we measure colours for inner and outer regions separately. We follow the method of Kelsey et al. (2021) and Kelsey et al. (2023), but use an elliptical aperture defined by DLR = 1 and an annulus with 1 < DLR < 4. Splitting on the colour of the region the SN occurred in (i.e., inner colour for SNe with $d_{\mathrm{DLR}} \leq 1$ and outer colour for SNe with $d_{\mathrm{DLR}} > 1$) makes negligible difference to the size of the step compared to the global colour.

To assess whether the Hubble residual step at $d_{\mathrm{DLR}} = 0.5$ is caused by the transition between older and younger stellar populations, we also plot Hubble residual versus d_{DLR} for SNe in blue regions and red regions. We compare this to the trend between the mass step and d_{DLR} in Fig. 7.

3.3 Inclination effects

Our d_{DLR} measurements give a projected normalised galactocentric SN distance, and therefore present a lower limit to the true (deprojected) galactocentric distance. This means that while SNe at high d_{DLR} are likely to truly be located in the outer regions, SNe with lower d_{DLR} can be more ambiguous. If galactocentric distance does influence the SN Ia Hubble residual, this effect may be diluted due to our (unavoidable) use of projected separation.

We investigate this effect by calculating the apparent eccentricity, e_{gal}, of each host galaxy as

$$e_{\mathrm{gal}} = \sqrt{1 - \frac{B^2}{A^2}}\,. \qquad (5)$$

We then identify a sample with $e_{\mathrm{gal}} < 0.5$ that has smaller inclinations (i.e., that are more face on galaxies), and limit our inner region sample to only those host galaxies.

The magnitude of the host mass step in this sample remains consistent at 0.095 ± 0.023 mag, while the significance decreases to 4.0σ due to the smaller sample size. We conclude that there is no evidence that inclination is affecting the d_{DLR} results.

4 DISCUSSION

We have uncovered a relationship between the Hubble residuals of SNe Ia and the projected, normalized galactocentric distance of the SN from its host galaxy. After standardization for stretch and colour, SNe Ia in the inner regions of their host galaxies ($d_{\mathrm{DLR}} \leq 0.5$) have more negative Hubble residuals (i.e., appear brighter) than those at moderate ($0.5 < d_{\mathrm{DLR}} \leq 1$) galactocentric distances (Fig. 4). More significantly, we have found that the magnitude of the step in Hubble residuals that occurs at stellar masses around $10^{10}\,\mathrm{M}_\odot$ is dependent upon the galactocentric distance: the step is large for SNe Ia with $d_{\mathrm{DLR}} \leq 1$ but negligible for SNe Ia with $d_{\mathrm{DLR}} > 1$ (Fig. 5).

Two leading astrophysical explanations for the host mass step are dust along the line of sight to the SN, and SN Ia progenitor age (or a combination of both). Here we discuss the implications of our findings for each model.

4.1 Dust

Previous studies have proposed an explanation of the host mass step in the form of a change in the ratio of total-to-selective extinction of the dust (R_V) in low and high-mass galaxies (Brout & Scolnic 2021). A key motivation for the introduction of the Brout & Scolnic (2021) model is that it can naturally explain the observation that the size of the mass step increases for redder SNe Ia. This trend between mass step size and SN colour is present (before the BBC 4D bias correction) in DES-SN5YR data (Vincenzi et al. 2024), as well as the Pantheon+ (Brout et al. 2022) and Amalgame (Popovic et al. 2024b) compilations, although the trend is not significant in the low-z ZTF sample (Ginolin et al. 2024b).

R_V determines the amount of dimming at a given wavelength for a total amount of reddening. Consider two populations of SNe with different dust screens: the two populations can experience the same distribution of reddening (i.e., the τ_E for each dust screen is identical) while experiencing different amounts of (for example) rest-frame B-band extinction if the average R_V is different. This difference in the extinction experienced in the rest-frame B-band (Δm_B) is quantified by

$$\Delta m_B = (R_V + 1)E(B - V)\,. \qquad (6)$$

If the R_V distributions are different for the two populations, the size of the difference in m_B, and thus Hubble residuals through equation 1, increases with increasingly red SN colours. Note that to explain the step, the extinction R_V must be larger in high-mass galaxies (opposite to trends observed in star-forming galaxies (Salim et al. 2018)) and passive galaxies (which follows the trend observed in that paper). Thorough investigations of the relationships between extinction R_V and attenuation R_V in the context of SN Ia cosmology can be found in Duarte et al. (2023) and Popovic et al. (2024a).

The difference between the observed mass step in inner and outer regions could be due to either a complete lack of dust in the outer regions of galaxies (i.e., there are no SNe with sufficiently large $E(B - V)$ to be affected by a difference in R_V) and/or a lack of evolution of the dust laws in the outskirts as galaxies transition from low to high mass (i.e, the R_V distribution is consistent in the outskirts of all galaxies). The signature of the former would be a deficiency of red SNe from the overall SN colour distribution in the outer regions compared to the inner regions. The latter would show up when plotting Hubble residual, split between high and low-mass hosts, against SN colour: inner regions would show diverging Hubble residuals for redder SNe, while outer regions would show no difference in the size of step as a function of SN colour. An evolution of the dust law may
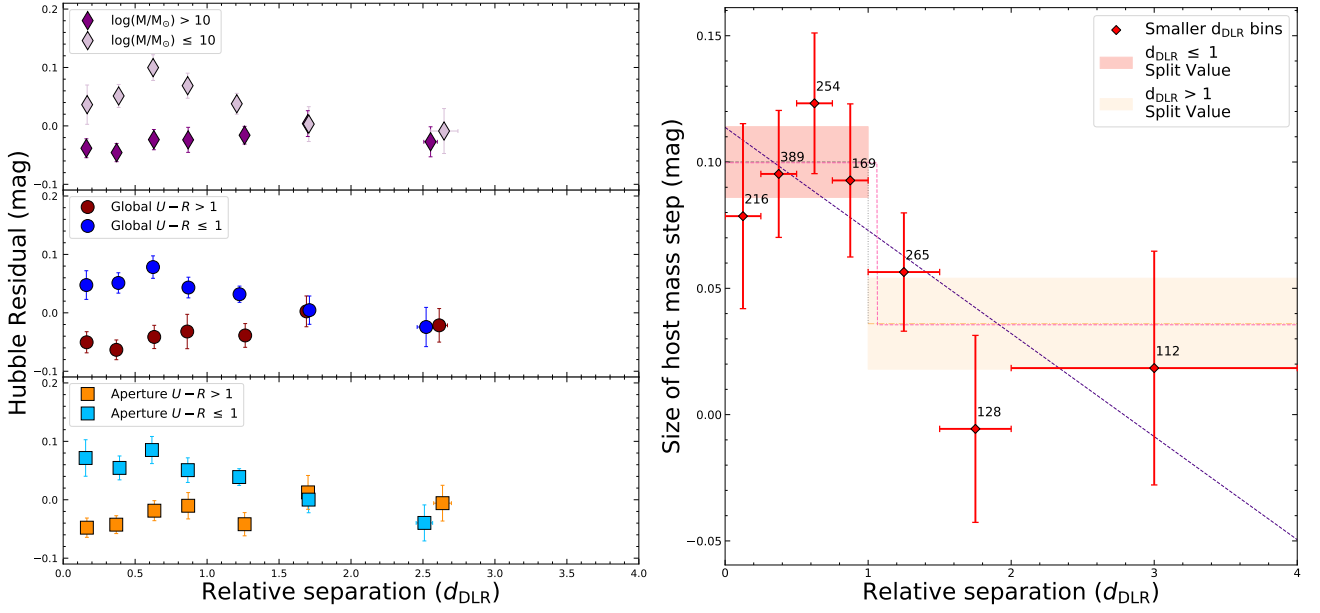
Figure 7. The host mass step observed in smaller d_{DLR} bins of 0.25 dex over $0 \leq d_{DLR} \leq 1$, 0.5 dex over $1 < d_{DLR} \leq 2$, and 2 dex at $d_{DLR} > 2$. Left: The Hubble residuals split into low and high stellar mass samples (top panel), split by the global host galaxy rest-frame $U - R$ colour (middle panel), and split by an aperture $U - R$ colour (lower panel). The aperture colours are described in Section 3.2.3. Right: The magnitude of the host mass step in these d_{DLR} bins. We fit both a step function and a linear function to our data, and find both have similar goodness-of-fit values. Numbers show the number of SNe Ia within each d_{DLR} bin.
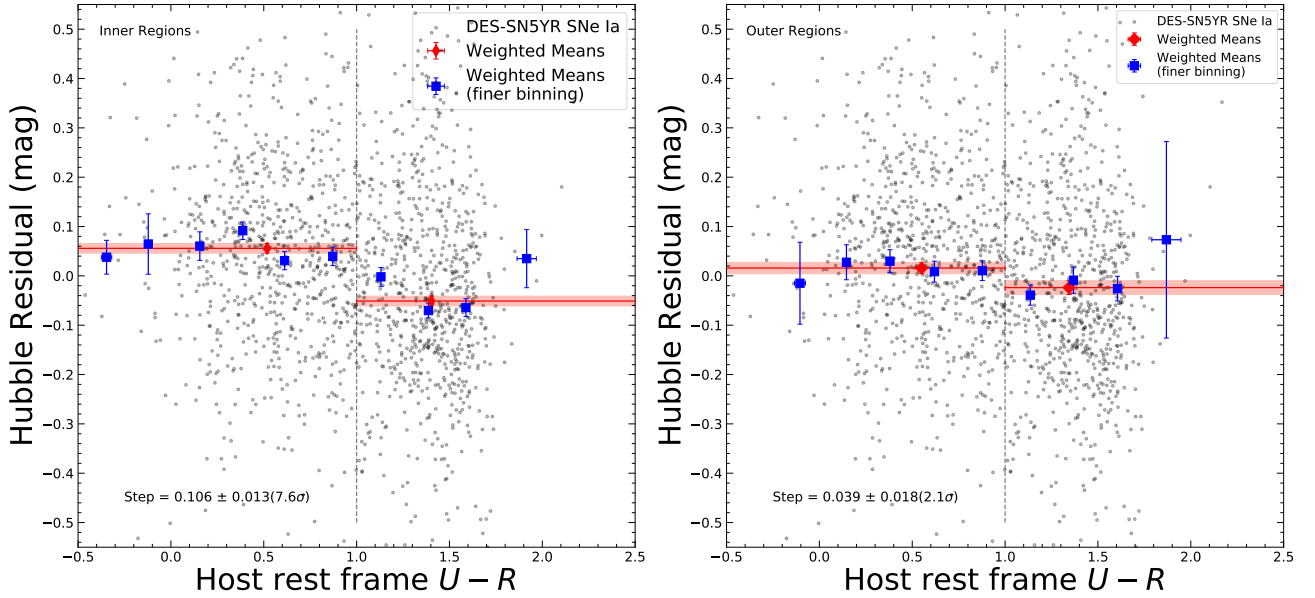
Figure 8. As Fig. 5 but for host galaxy rest-frame $U - R$ colour. The step sizes are 0.106 ± 0.013 mag (left) and 0.039 ± 0.018 mag (right).

also present as a difference in the best-fitting β values from Eq. 1 between the high and low-mass samples in our two regions, because of the contribution of Eq. 6 to the overall colour–luminosity relation β. We next investigate these possibilities.

4.1.1 SN colour distributions

We perform two-sample statistical tests to determine whether the colour distributions are different. The SALT3 c distributions for SNe in inner ($d_{DLR} \leq 1$) and outer ($d_{DLR} > 1$) regions (Fig. 9) are

consistent with being sampled from the same parent distribution: the two-sided Kolmogorov–Smirnov (KS) test statistic is 0.05 with a $p = 0.29$, while a Mann–Whitney U test results in $p = 0.12$. However, when splitting instead at $d_{DLR} = 1.5$, we find with high significance that the samples come from different populations (KS $p = 5.6 \times 10^{-4}$, Mann–Whitey U $p = 1.9 \times 10^{-3}$).

To test whether this effect is caused by selection effects, we define a 'colour test' sample. We limit the redshift to $z < 0.6$ to retain higher quality light-curves, while relaxing the SN colour selection of the cosmological sample and allowing the reddest SNe Ia up to

Table 3. Best-fitting parameters for the intrinsic + dust colour model. DES-SN5YR is the nominal sample (no redshift selection, but with x_1 and c restricted as in Vincenzi et al. (2024). In the middle section we loosen the c selection from $-0.3 < c < 0.3$ to $-0.5 < c < 0.5$, and select SNe Ia with $z < 0.6$. The lower section shows the Ginolin et al. (2024b) ZTF results.

Selection	μ_c	σ_c	τ_E
DES-SN5YR; nominal	-0.057 ± 0.003	0.038 ± 0.003	0.093 ± 0.004
$d_{\mathrm{DLR}} \leq 1$	-0.056 ± 0.003	0.038 ± 0.003	0.100 ± 0.005
$d_{\mathrm{DLR}} > 1$	-0.056 ± 0.004	0.034 ± 0.003	0.093 ± 0.007
$d_{\mathrm{DLR}} \leq 1.5$	-0.054 ± 0.003	0.037 ± 0.003	0.100 ± 0.005
$d_{\mathrm{DLR}} > 1.5$	-0.062 ± 0.004	0.030 ± 0.003	0.070 ± 0.007
DES-SN5YR; $z < 0.6$, $|c| < 0.5$	-0.048 ± 0.003	0.034 ± 0.003	0.127 ± 0.006
$d_{\mathrm{DLR}} \leq 1$	-0.047 ± 0.003	0.036 ± 0.003	0.132 ± 0.007
$d_{\mathrm{DLR}} > 1$	-0.050 ± 0.004	0.035 ± 0.004	0.115 ± 0.009
$d_{\mathrm{DLR}} \leq 1.5$	-0.046 ± 0.003	0.037 ± 0.003	0.131 ± 0.007
$d_{\mathrm{DLR}} > 1.5$	-0.056 ± 0.004	0.030 ± 0.004	0.093 ± 0.009
ZTF Ginolin et al. (2024b) Full sample	-0.086 ± 0.004	0.029 ± 0.005	0.157 ± 0.007
ZTF Ginolin et al. (2024b) Dustless sample	-0.092 ± 0.008	0.032 ± 0.008	0.099 ± 0.011
ZTF Ginolin et al. (2024b) Non dustless sample	-0.081 ± 0.005	0.029 ± 0.006	0.168 ± 0.008
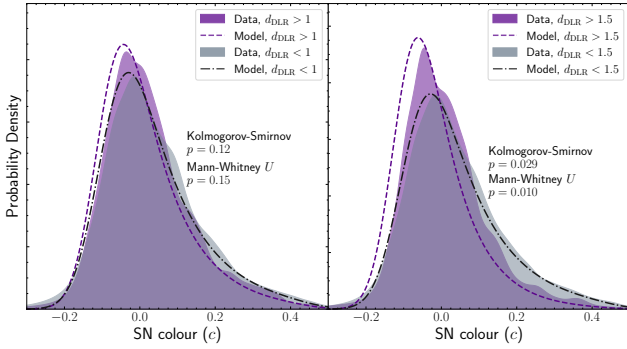
Figure 9. Left: SALT3 colour (c) distributions for SNe in inner ($d_{\mathrm{DLR}} \leq 1$, grey) and outer ($d_{\mathrm{DLR}} > 1$, purple) regions, for a 'colour test' sample with $z < 0.6$ and SN $c < 0.5$. The overplotted models are the best-fitting intrinsic distributions, broadened by a uniform smear equal to the average uncertainty in the data. We find there is no significant difference between the samples. Right: As left, but when splitting at $d_{\mathrm{DLR}} = 1.5$. In this case there is a strong difference between the two colour distributions.

$c < 0.5$ to probe the full reddening tail. This gives 1268 SNe Ia. We repeat the tests, and the results are similar after having made this selection.

Interestingly, if instead we split the samples at $d_{\mathrm{DLR}} = 1.5$, we find that the samples are significantly different, both in the nominal DES-SN5YR and the 'colour test' selections. This result indicates that SNe Ia at $d_{\mathrm{DLR}} > 1.5$ are less affected by reddening, and is consistent with the findings of Ginolin et al. (2024b)[2], but does not explain why $d_{\mathrm{DLR}} = 1$ is the point at which there is the most significant difference in mass steps.

To further investigate these results we fit our data with the commonly used functional form as in Jha et al. (2007), Mandel et al. (2011), and Brout & Scolnic (2021), where the intrinsic colour distribution is modelled by a Gaussian (mean μ_c, width σ_c), with red-

---

[2] Note that DLR is defined differently between ZTF and DES, with ZTF defining DLR=1 as the half-light radius, which is roughly DLR=0.68 in DES; thus the ZTF choice of $d_{\mathrm{DLR}} > 1.5$ for dustless SNe Ia is consistent with our split of $d_{\mathrm{DLR}} = 1$.

dening introducing an exponential tail of scale τ_E. This exponential follows the expected distribution of reddening within the disk of late-type galaxies (Hatano et al. 1998; Commins 2004; Riello & Patat 2005). We follow Ginolin et al. (2024b) in fitting the model directly to the data (without binning and fitting to a histogram), by evaluating the likelihood of each colour observation given the model and the uncertainty of the colour measurements, and minimizing the sum of the negative log-likelihood (equation 1 in Ginolin et al. 2024b).

The results are presented in Table 3, and the example of the model fitted to the 'colour test' sample is shown in Fig. 9. As above, when splitting the DES-SN5YR sample at $d_{\mathrm{DLR}} = 1$ we find μ_c, σ_c and τ_E are consistent between SNe Ia in the inner and outer regions, inconsistent with the results from Ginolin et al. (2024b) where τ_E is reduced by ~ 30 per cent in the outer regions. We find consistent parameters even when limiting to the 'colour test' sample. Once more, if we split at $d_{\mathrm{DLR}} = 1.5$ we find τ_E is significantly larger in outer regions, with the difference between inner and outer regions enhanced in the 'colour test' sample. No matter our selection, the DES data are not fit by as large a τ_E as the low-z ZTF Ginolin et al. (2024b) sample, due to selection effects, choice of light curve fitter, and possible redshift evolution. Therefore direct comparisons between the colour distributions are not meaningful.

4.1.2 Hubble residuals as a function of SN Ia colour

Given the consistency of the SN Ia colour distributions between SNe Ia in inner and outer regions (Section 4.1.1), we now consider the slope of the dust extinction laws as a possible reason for the difference in step size.

The Hubble residuals are plotted against SN Ia colour for inner and outer regions in the left and right hand panels of Fig. 10 respectively. In inner regions, the mass step for all colours redder than $c = -0.1$ is clear, and increases with increasing colour: this is consistent with what was seen in the full DES-SN5YR sample (Kelsey et al. 2023; Vincenzi et al. 2024). The step in blue SNe Ia is not explained well by differing R_V distributions and has been attributed to SNe Ia from differing ages of stellar population (Kelsey et al. 2023; Wiseman et al. 2022; Popovic et al. 2024a). The step in blue SNe Ia in inner regions, but not in outer regions, may be explained by a more diverse stellar (and SN progenitor) population in the inner regions of galaxies, while

Table 4. Strength of the SN Ia colour–luminosity relation β (equation 1) for SNe Ia in different host galaxy environments.

Sample	β
Full Sample	2.72 ± 0.05
$d_{\mathrm{DLR}} \leq 1$	2.72 ± 0.08
$d_{\mathrm{DLR}} > 1$	2.73 ± 0.07
$\log(M_*/\mathrm{M}_\odot) \leq 10$	2.96 ± 0.09
$\log(M_*/\mathrm{M}_\odot) > 10$	2.66 ± 0.05
$d_{\mathrm{DLR}} \leq 1$	
$\log(M_*/\mathrm{M}_\odot) \leq 10$	2.94 ± 0.11
$\log(M_*/\mathrm{M}_\odot) > 10$	2.67 ± 0.06
$d_{\mathrm{DLR}} > 1$	
$\log(M_*/\mathrm{M}_\odot) \leq 10$	2.89 ± 0.16
$\log(M_*/\mathrm{M}_\odot) > 10$	2.69 ± 0.09

the outer regions host a homogeneous population of SNe Ia regardless of the host mass. We can invoke a similar description for dust: inner regions evolve such that their average dust laws are different for host galaxies of different mass, while outer regions retain the same dust properties throughout the evolution of the galaxy as a whole.

We additionally calculate the slope of the colour-luminosity relation (β) for each of our subsamples (split at $d_{\mathrm{DLR}} = 1$), shown in Fig. 11 and Table. 4. There is no overall difference between β in inner and outer regions, but a significant difference ($\Delta\beta = 0.3$; $2.8\,\sigma$) between low and high-mass galaxies in general (Sullivan et al. 2010; Brout & Scolnic 2021; Chen et al. 2022). This difference is weakened ($\Delta\beta = 0.27$; $2.2\,\sigma$) in inner regions, and the significance is reduced further in outer regions ($\Delta\beta = 0.2$; $1.1\,\sigma$) as the sample size is much smaller. We find that SNe within the inner regions of their host are best fit with different β values between high and low-mass hosts. Within the outer regions however, there is no significant difference between high and low-mass β.

In Fig. 12 we show the standardized Hubble residuals after performing a BBC 4D bias correction which assumes a different R_V distribution for low and high-mass galaxies. In inner regions, the characteristic curve of Hubble residual from blue to red SNe is removed, as is the differential difference between low and high-mass galaxies. However, a difference of ~ 0.04 mag between low and high-mass hosts remains at all colours, as discussed in Vincenzi et al. (2024). In outer regions, the curve is also removed but no significant residual difference exists at any SN colour.

4.2 Populations of SN Ia progenitors

A difference in the effects of dust extinction between inner and outer regions does not seem to be the cause of the difference in host galaxy steps between those regions. A different explanation could be that the SN explosions themselves occur in multiple progenitors, with a different average standardized peak brightness. These populations are then present in differing proportions between the inner regions of low-mass/blue/young and high-mass/red/old galaxies, but the outer regions of all galaxies only host a single population.

These progenitors are often assumed to relate to the 'delay time' from an initial burst of star formation to the SN Ia explosion. For the SN Ia population as a whole, the distribution of these delay times – the delay time distribution (DTD) – is well described by a declining power law (Maoz & Gal-Yam 2004; Totani et al. 2008; Maoz et al. 2010, 2014; Graur et al. 2015; Castrillo et al. 2021; Wiseman et al. 2021). When such a DTD is convolved with the stellar age distribution

of stars across different galaxy types, a bimodal distribution for the age of SN progenitors at the time of explosion is observed (Mannucci et al. 2005; Scannapieco & Bildsten 2005; Mannucci et al. 2006; Sullivan et al. 2006; Smith et al. 2012; Childress et al. 2014; Wiseman et al. 2021): so-called 'prompt' and 'delayed' components.

Rigault et al. (2013) and Childress et al. (2014) proposed that if a difference in average peak brightness of the prompt and delayed populations is the cause of the step, then the step size should change as a function of redshift. Evidence for such an evolution is limited, although we note the step observed in the high-z DES-SN5YR sample (before dust-like bias corrections) is somewhat smaller than that seen in the low-z ZTF sample (Ginolin et al. 2024b). There is, however, strong evidence that these populations do have different light curve characteristics. Their stretch distributions are different, with faster declining light curves (lower x_1) occurring more frequently in environments with older, more passive stellar populations (e.g., Hamuy et al. 1995; Sullivan et al. 2006).

Recent analyses observe two distinct 'modes' of SN stretch: a low-stretch mode which is observed only in passive environments, and a high-stretch mode observed in both star-forming and passive environments (e.g., Rigault et al. 2020). Nicolas et al. (2021) showed that the relative abundance of these modes in an observed population of SNe Ia evolves as a function of redshift, which can be explained if the modes relate to the prompt and delayed modes of the SN Ia DTD. What is not clear is whether the two modes have different standardized peak brightnesses, or require different standardization parameters α and β.

We test whether there is a difference in the SN Ia populations between the inner and outer regions by modelling the x_1 distributions according to the Nicolas et al. (2021) model. By using the annulus colour as a proxy for the age of the stellar population, we fix their y^i parameter, which is the probability that the progenitor is young, according to

$$y^i = \begin{cases} 1, & (U-R)_{\mathrm{annulus}} < 1 \\ 0, & (U-R)_{\mathrm{annulus}} \geq 1 \end{cases}. \tag{7}$$

The model for the x_1 distribution is then

$$p(x_1) \sim \begin{cases} \mathcal{N}(\mu_{1,x_1}, \sigma_{1,x_1}), & (U-R)_{\mathrm{annulus}} < 1 \\ a\mathcal{N}(\mu_{1,x_1}, \sigma_{1,x_1}) + \\ (1-a)\mathcal{N}(\mu_{2,x_1}, \sigma_{2,x_1}), & (U-R)_{\mathrm{annulus}} > 1 \end{cases}. \tag{8}$$

The parameter a determines the fraction of high-stretch mode SNe occurring in the delayed stellar population.

We fit the full dataset with this model by minimizing the negative log-likelihood, and show the data and best-fitting model in Fig 13. We find $\mu_{1,x_1} = 0.22 \pm 0.03$, $\sigma_{1,x_1} = 0.67 \pm 0.03$, $\mu_{2,x_1} = -0.86 \pm 0.17$, $\sigma_{2,x_1} = 0.80 \pm 0.07$, and $a = 0.37 \pm 0.1$ which are broadly consistent with the results of Nicolas et al. (2021) and Ginolin et al. (2024a) except for a which is significantly smaller than found in those works but consistent with the value for DES-SN5YR modelled in Wiseman et al. (2022). This small a could be caused by our fixing of y^i based on the galaxy colours: it is known that no galaxy observable perfectly traces the underlying properties, and even locally measured colours experience contamination whereby young SNe occur in populations measured to be old (Briday et al. 2022). If instead we fix the probability that any given SN is young to the average for our mean redshift according to the Rigault et al. (2020) drift model, $\delta(z = 0.53) = 0.67$, we find $\mu_{1,x_1} = 0.06$, $\sigma_{1,x_1} = 0.70$, $\mu_{2,x_1} = -1.65$, $\sigma_{2,x_1} = 0.45$, and $a = 0.58$. Note that these mean values are slightly more negative than the low-z values from Nicolas et al. (2021) and Ginolin et al. (2024a) – this could be genuine redshift evolution or an effect of the use of SALT2 rather than SALT3 light curve fits in those works.
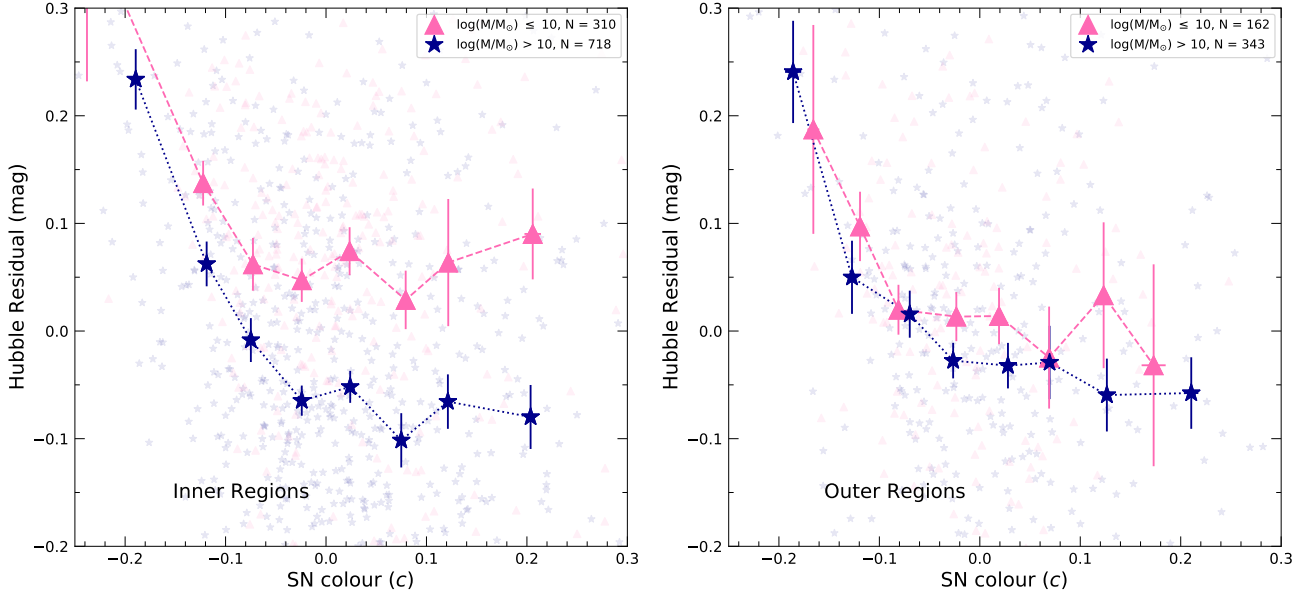
Figure 10. Hubble residuals for our inner (left) and outer (right) regions as a function of SALT3 colour c, plotted separately for events in low and high-mass host galaxies. The difference between the high- and low-mass points is effectively the mass step at any SN Ia colour.
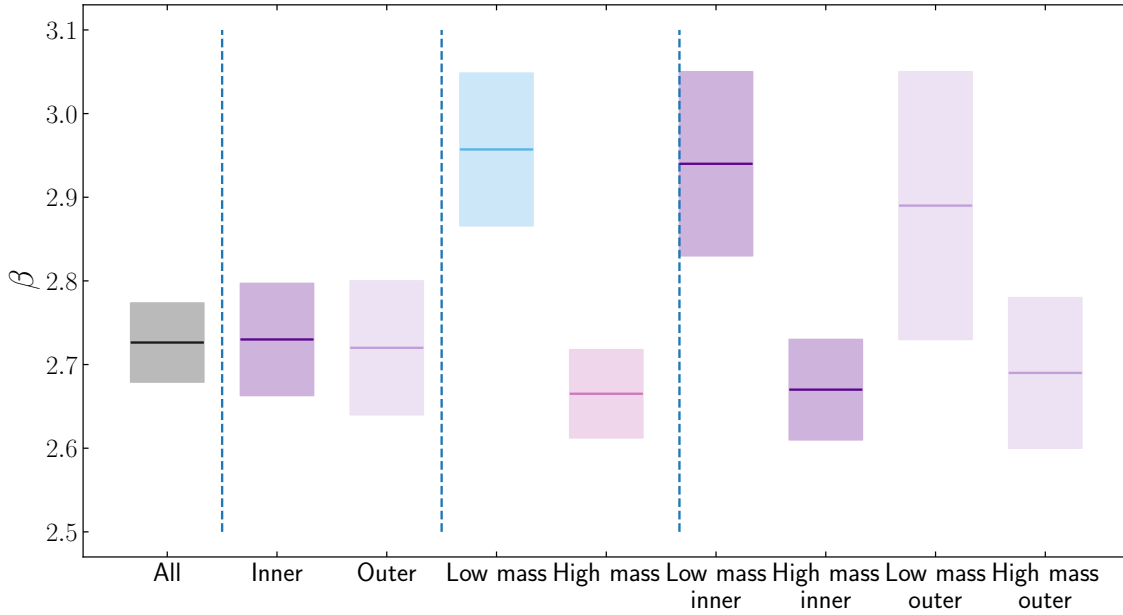

Figure 11. The strength of the colour–luminosity relationship parametrized by β, for different host galaxy selections. Our best-fitting estimates are represented by horizontal lines, with the 1 σ uncertainty shown as a shaded region.

Next, we fit the inner and outer SNe separately, fixing the model parameters to those found using the aperture/annulus colour as a proxy for stellar population age, except for a which we leave free. We find $a = 0.32 \pm 0.05$ in inner regions and $a = 0.42 \pm 0.04$ in outer regions, which means there is a larger fraction of high-stretch mode SNe in red outer annuli compared to red central regions.

The results of this test indicate that inner regions are more strongly split between the high-stretch SN mode in young and blue stellar populations and the low-stretch SN mode in old and red stellar populations. The outer regions have a more mixed population of low and high-stretch modes in their old and red stellar populations. If the Hubble residual step is caused by differences between these two
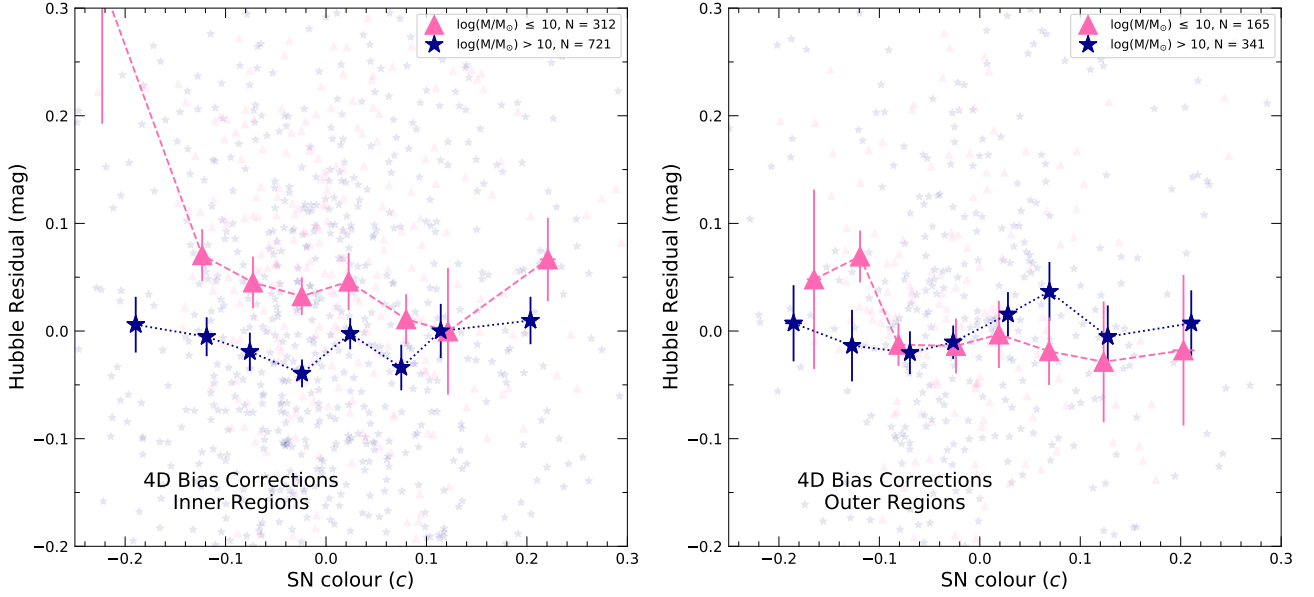
Figure 12. Hubble residuals for our inner (left) and outer (right) regions as a function of SALT3 colour c, plotted separately for events in low and high-mass host galaxies, after having made a BBC 4D correction for the colour-dependent selection and dust bias.
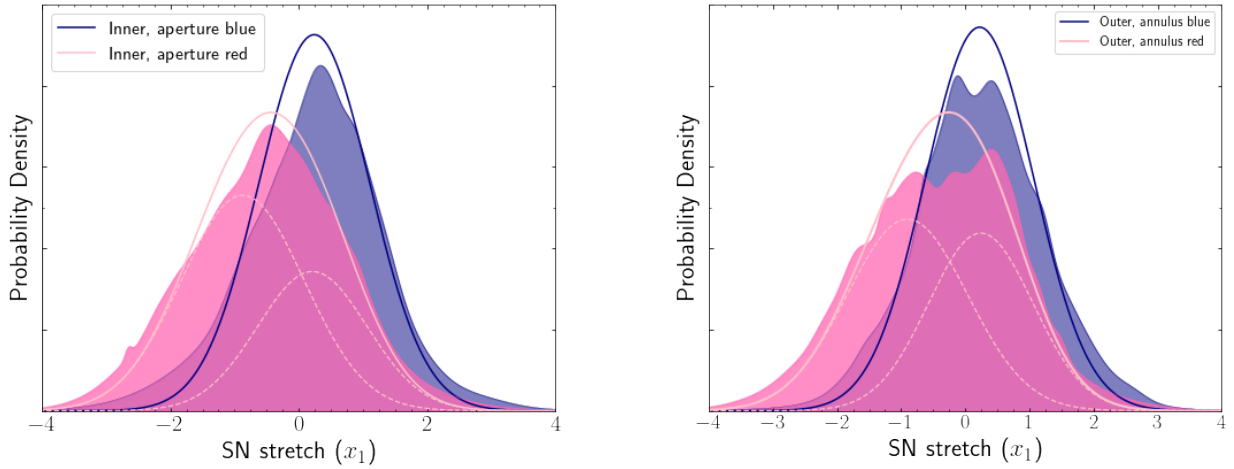
Figure 13. SN stretch distributions for the inner ($d_{DLR} \leq 1$) and outer ($d_{DLR} > 1$) regions, split according to the colour of the aperture/annulus of the location of the SN. The models plotted are results of fit directly to the data, and are drawn by adding a uniform smear equal to the mean x_1 uncertainty to the intrinsic width.

modes, then this difference could be a tangible explanation. In particular, Wiseman et al. (2022) noted that the inferred strength of the width-luminosity relation α is degenerate with a Hubble residual step that is related to the stellar age of the SN progenitor. If α is being mis-measured because it actually has a different strength for the two modes, this could introduce an artificial Hubble residual dependence that is related to the stellar population age.

However, Ginolin et al. (2024a) modelled their SN distances, standardized for colour but not stretch, with a two-component 'broken' α and found that while the standardization is improved, the host mass or host colour Hubble residual step *increases*. Furthermore, the difference between the Hubble residuals in inner and outer regions appears more driven by the low-mass and blue environments whose Hubble residuals become more negative in outer regions, while the high-mass and red environments are relatively unchanged. That is, the difference in Hubble residuals is insensitive to the relative fraction of low/high-stretch SNe in red/high-mass hosts.

4.3 Implications for cosmological measurements

Distance measurements using SNe Ia are at the forefront of cosmology due to an increase in sample sizes combined with an improved handling of systematics. In DES-SN5YR, the systematic uncertainty on the dark energy equation of state parameter w is smaller than the statistical uncertainty (Vincenzi et al. 2024). Nevertheless, the largest component of this systematic uncertainty is the colour-and-

host dependent scatter model and associated bias corrections. Given that the values used for the BBC-4D bias correction are conditioned on the full dataset, it could be that the corrections are underestimated in inner regions, and overestimated in outer regions. A full analysis of the impact of this effect is beyond the scope of this work. Here we note that for the effect to propagate through to a bias on w, it would require the distribution of d_{DLR} to evolve with redshift. Instead the d_{DLR} distribution remains constant as a function of redshift in DES-SN5YR.

5 SUMMARY

Using the DES five-year sample of photometrically-classified SNe Ia, we have analysed the effects of projected and normalized host galaxy separation on the light-curve properties and inferred cosmological distance measurements. Using the directional light radius (DLR) method as our normalisation of the galactocentric distances (d_{DLR}), our main findings are:

- We confirm previous findings of Toy et al. (2023) that the inner-most regions of galaxies ($d_{DLR} \leq 1$) host faster-declining SNe than the outer regions.
- We show, for the first time, that the difference in SN Ia post-standardization brightnesses between high and low-mass hosts reduces from 0.078 ± 0.011 mag in the full sample to 0.036 ± 0.018 mag for SNe Ia located in the outer regions of their host galaxies ($d_{DLR} > 1$), while increasing to 0.100 ± 0.014 mag for SNe in the inner regions ($d_{DLR} \leq 1$). The effect remains when splitting SNe Ia by their global galaxy $U - R$ colour, or by the $U - R$ colour in the inner aperture/outer annulus in which the SN occurred.
- We find that the decrease in magnitude of this mass step as a function of d_{DLR} is well fit by either a step function, split at d_{DLR} of 1, or a linear function with d_{DLR}.
- We show that using different R_V values for dust along the line of sight to SNe that varies between low and high-mass host galaxies, can reduce but not remove the step for SNe Ia in the inner regions.
- There is no evidence that the outer regions of galaxies have dust laws that change as a function of stellar mass. Similarly, there is no evidence for an intrinsic luminosity difference between SNe Ia in the outer regions of low and high-mass galaxies.
- We find a slight difference between the strength of the high-stretch mode of SN Ia x_1 in red inner and red outer regions, but consider this effect unlikely to be the cause of the Hubble residual effect.

Calculating d_{DLR} is an algorithmically straight forward task, and selecting SNe Ia based on d_{DLR} reduces the need to account for host galaxy properties to standardize SN Ia brightnesses across different galaxies, without much computational effort. While we have not identified the underlying astrophysics that such projected galactocentric distances are tracing in the DES five-year SN Ia sample, we have shown that the standardized distance measurements from SNe Ia in the outer regions of galaxies have little dependence on their global host galaxy properties.

Restricting a cosmological analysis to SNe Ia in the outer regions of their host galaxies reduces the sample size to around a third. This will increase the statistical uncertainties. However, the reduction in the astrophysical systematic uncertainties (and complications) gained from using such a sample, coupled with the very large sample sizes expected in future experiments such as the Rubin Observatory's Legacy Survey of Space and Time (LSST) (Ivezić et al. 2019), means that such a selection is likely to be beneficial.

DATA AVAILABILITY

All data used in this article are publicly available with the DES-SN5YR data release (Sánchez et al. 2024) at `https://github.com/des-science/DES-SN5YR`.

REFERENCES

Anderson J. P., James P. A., Förster F., González-Gaitán S., Habergham S. M., Hamuy M., Lyman J. D., 2015, MNRAS, 448, 732
Astier P., et al., 2006, A&A, 447, 31
Baes M., Sil'chenko O. K., Moiseev A. V., Manakova E. A., 2007, A&A, 467, 991
Bertin E., Arnouts S., 1996, A&AS, 117, 393
Bessell M. S., 1990, PASP, 102, 1181
Betoule M., et al., 2014, A&A, 568, A22
Briday M., et al., 2022, A&A, 657, A22
Brout D., Scolnic D., 2021, ApJ, 909, 26
Brout D., 2022, ApJ, 938, 110
Castrillo A., et al., 2021, MNRAS, 501, 3122
Chen R., et al., 2022, ApJ, 938, 62
Childress M., et al., 2013, ApJ, 770, 108
Childress M. J., Wolf C., Zahid H. J., 2014, MNRAS, 445, 1898
Commins E. D., 2004, New Astron. Rev., 48, 567
Conley A., et al., 2008, ApJ, 681, 482
DES Collaboration et al., 2024, arXiv e-prints, p. arXiv:2401.02929
Duarte J., et al., 2023, A&A, 680, A56
Galbany L., et al., 2012, ApJ, 755, 125
Ginolin M., et al., 2024a, arXiv e-prints, p. arXiv:2405.20965
Ginolin M., et al., 2024b, arXiv e-prints, p. arXiv:2406.02072
Goddard D., et al., 2017, MNRAS, 466, 4731
González Delgado R. M., et al., 2014, ApJ, 791, L16
González Delgado R. M., et al., 2015, A&A, 581, A103
Graur O., Bianco F. B., Modjaz M., 2015, MNRAS, 450, 905
Gupta R. R., et al., 2016, AJ, 152, 154
Guy J., et al., 2007, A&A, 466, 11
Hamuy M., Phillips M. M., Maza J., Suntzeff N. B., Schommer R. A., Aviles R., 1995, AJ, 109, 1
Hamuy M., Trager S. C., Pinto P. A., Phillips M. M., Schommer R. A., Ivanov V., Suntzeff N. B., 2000, AJ, 120, 1479
Hatano K., Branch D., Deaton J., 1998, ApJ, 502, 177
Hayden B. T., Gupta R. R., Garnavich P. M., Mannucci F., Nichol R. C., Sako M., 2013, ApJ, 764, 191
Hicken M., Wood-Vasey W. M., Blondin S., Challis P., Jha S., Kelly P. L., Rest A., Kirshner R. P., 2009, ApJ, 700, 1097
Hill R., et al., 2018, MNRAS, 481, 2766
Hsiao E. Y., Conley A., Howell D. A., Sullivan M., Pritchet C. J., Carlberg R. G., Nugent P. E., Phillips M. M., 2007, ApJ, 663, 1187
Ivanov V. D., Hamuy M., Pinto P. A., 2000, ApJ, 542, 588
Ivezić Ž., et al., 2019, ApJ, 873, 111
Jha S., Riess A. G., Kirshner R. P., 2007, ApJ, 659, 122
Johnson H. L., Morgan W. W., 1953, ApJ, 117, 313
Jones D. O., et al., 2018a, ApJ, 857, 51

Jones D. O., et al., 2018b, ApJ, 867, 108
Kelly P. L., Hicken M., Burke D. L., Mandel K. S., Kirshner R. P., 2010, ApJ, 715, 743
Kelsey L., et al., 2021, MNRAS, 501, 4861
Kelsey L., et al., 2023, MNRAS, 519, 3046
Kenworthy W. D., et al., 2021, ApJ, 923, 265
Kessler R., Scolnic D., 2017, ApJ, 836, 56
Kessler R., et al., 2009, ApJS, 185, 32
Kessler R., et al., 2015, AJ, 150, 172
Kormendy J., Djorgovski S., 1989, ARA&A, 27, 235
Lampeitl H., et al., 2010, ApJ, 722, 566
Lidman C., et al., 2020, MNRAS, 496, 19
Maiolino R., Mannucci F., 2019, A&ARv, 27, 3
Malmquist K. G., 1922, Meddelanden fran Lunds Astronomiska Observatorium Serie I, 100, 1
Malmquist K. G., 1925, Meddelanden fran Lunds Astronomiska Observatorium Serie I, 106, 1
Mandel K. S., Narayan G., Kirshner R. P., 2011, ApJ, 731, 120
Mannucci F., Della Valle M., Panagia N., Cappellaro E., Cresci G., Maiolino R., Petrosian A., Turatto M., 2005, A&A, 433, 807
Mannucci F., Della Valle M., Panagia N., 2006, MNRAS, 370, 773
Maoz D., Gal-Yam A., 2004, MNRAS, 347, 951
Maoz D., Sharon K., Gal-Yam A., 2010, ApJ, 722, 1879
Maoz D., Mannucci F., Nelemans G., 2014, ARA&A, 52, 107
Millán-Irigoyen I., del Valle-Espinosa M. G., Fernández-Aranda R., Galbany L., Gomes J. M., Moreno-Raya M., López-Sánchez Á. R., Mollá M., 2022, MNRAS, 517, 3312
Möller A., de Boissière T., 2020, MNRAS, 491, 4277
Möller A., et al., 2022, MNRAS, 514, 5159
Moreno-Raya M. E., Mollá M., López-Sánchez Á. R., Galbany L., Vílchez J. M., Carnero Rosell A., Domínguez I., 2016, ApJ, 818, L19
Nicolas N., et al., 2021, A&A, 649, A74
Nugent A. E., Polin A. E., Nugent P. E., 2023, arXiv e-prints, p. arXiv:2304.10601
Pagel B. E. J., Edmunds M. G., 1981, ARA&A, 19, 77
Pan Y. C., Sullivan M., Maguire K., Gal-Yam A., Hook I. M., Howell D. A., Nugent P. E., Mazzali P. A., 2015, MNRAS, 446, 354
Parikh T., Thomas D., Maraston C., Westfall K. B., Andrews B. H., Boardman N. F., Drory N., Oyarzun G., 2021, MNRAS, 502, 5508
Perlmutter S., et al., 1997, ApJ, 483, 565
Perrett K., et al., 2010, AJ, 140, 518
Phillips M. M., 1993, ApJ, 413, L105
Popovic B., Brout D., Kessler R., Scolnic D., Lu L., 2021, ApJ, 913, 49
Popovic B., Brout D., Kessler R., Scolnic D., 2023, ApJ, 945, 84
Popovic B., et al., 2024a, arXiv e-prints, p. arXiv:2406.05051
Popovic B., et al., 2024b, MNRAS, 529, 2100
Qu H., et al., 2024, ApJ, 964, 134
Riello M., Patat F., 2005, MNRAS, 362, 671
Riess A. G., Press W. H., Kirshner R. P., 1996, ApJ, 473, 88
Rigault M., et al., 2013, A&A, 560, A66
Rigault M., et al., 2020, A&A, 644, A176
Roman M., et al., 2018, A&A, 615, A68
Rose B. M., Garnavich P. M., Berg M. A., 2019, ApJ, 874, 32
Sako M., et al., 2018, PASP, 130, 064002
Salim S., Boquien M., Lee J. C., 2018, ApJ, 859, 11
Sánchez S. F., et al., 2014, A&A, 563, A49
Sánchez B. O., et al., 2024, arXiv e-prints, p. arXiv:2406.05046
Scannapieco E., Bildsten L., 2005, ApJ, 629, L85
Scolnic D., Kessler R., 2016, ApJ, 822, L35
Searle L., 1971, ApJ, 168, 327
Sérsic J. L., 1963, Boletin de la Asociacion Argentina de Astronomia La Plata Argentina, 6, 41
Simpson J. P., Colgan S. W. J., Rubin R. H., Erickson E. F., Haas M. R., 1995, ApJ, 444, 721
Smith M., et al., 2012, ApJ, 755, 61
Smith M., et al., 2020, MNRAS, 494, 4426
Stobie R. S., 1980, in Elliott D. A., ed., Society of Photo-Optical Instrumentation Engineers (SPIE) Conference Series Vol. 264, Conference on

Applications of Digital Image Processing to Astronomy. pp 208–212, doi:10.1117/12.959806

Sullivan M., et al., 2006, ApJ, 648, 868

Sullivan M., et al., 2010, MNRAS, 406, 782

Taylor G., et al., 2023, MNRAS, 520, 5209

Thorp S., Mandel K. S., 2022, MNRAS, 517, 2360

Totani T., Morokuma T., Oda T., Doi M., Yasuda N., 2008, PASJ, 60, 1327

Toy M., et al., 2023, MNRAS, 526, 5292

Tripp R., 1998, A&A, 331, 815

Uddin S. A., et al., 2020, ApJ, 901, 143

Vincenzi M., et al., 2024, arXiv e-prints, p. arXiv:2401.02945

Wang X., Wang L., Filippenko A. V., Zhang T., Zhao X., 2013, Science, 340, 170

Wiseman P., et al., 2020, MNRAS, 495, 4040

Wiseman P., et al., 2021, MNRAS, 506, 3330

Wiseman P., et al., 2022, MNRAS, 515, 4587

Wiseman P., Sullivan M., Smith M., Popovic B., 2023, MNRAS, 520, 6214

Yasuda N., Fukugita M., 2010, AJ, 139, 39

[1] School of Physics and Astronomy, University of Southampton, Southampton, SO17 1BJ, UK

[2] Department of Physics, Duke University Durham, NC 27708, USA

[3] Einstein Fellow

[4] Department of Physics, University of Oxford, Denys Wilkinson Building, Keble Road, Oxford OX1 3RH, United Kingdom

[5] Center for Astrophysics | Harvard & Smithsonian, 60 Garden Street, Cambridge, MA 02138, USA

[6] School of Mathematics and Physics, University of Queensland, Brisbane, QLD 4072, Australia

[7] Institut d'Estudis Espacials de Catalunya (IEEC), 08034 Barcelona, Spain

[8] Institute of Space Sciences (ICE, CSIC), Campus UAB, Carrer de Can Magrans, s/n, 08193 Barcelona, Spain

[9] Centre for Gravitational Astrophysics, College of Science, The Australian National University, ACT 2601, Australia

[10] The Research School of Astronomy and Astrophysics, Australian National University, ACT 2601, Australia

[11] Department of Physics and Astronomy, University of Pennsylvania, Philadelphia, PA 19104, USA

[12] Institute of Cosmology and Gravitation, University of Portsmouth, Portsmouth, PO1 3FX, UK

[13] Department of Astronomy and Astrophysics, University of Chicago, Chicago, IL 60637, USA

[14] Kavli Institute for Cosmological Physics, University of Chicago, Chicago, IL 60637, USA

[15] Centre for Astrophysics & Supercomputing, Swinburne University of Technology, Victoria 3122, Australia

[16] Université Grenoble Alpes, CNRS, LPSC-IN2P3, 38000 Grenoble, France

[17] Department of Physics & Astronomy, University College London, Gower Street, London, WC1E 6BT, UK

[18] Physics Department, Lancaster University, Lancaster, LA1 4YB, UK

[19] Fermi National Accelerator Laboratory, P. O. Box 500, Batavia, IL 60510, USA

[20] Laboratório Interinstitucional de e-Astronomia - LIneA, Rua Gal. José Cristino 77, Rio de Janeiro, RJ - 20921-400, Brazil

[21] Department of Physics, University of Michigan, Ann Arbor, MI 48109, USA

[22] Kavli Institute for Particle Astrophysics & Cosmology, P. O. Box 2450, Stanford University, Stanford, CA 94305, USA

[23] SLAC National Accelerator Laboratory, Menlo Park, CA 94025, USA

[24] Instituto de Astrofisica de Canarias, E-38205 La Laguna, Tenerife, Spain

[25] Institut de Física d'Altes Energies (IFAE), The Barcelona Institute of Science and Technology, Campus UAB, 08193 Bellaterra (Barcelona) Spain

[26] Hamburger Sternwarte, Universität Hamburg, Gojenbergsweg 112, 21029 Hamburg, Germany

[27] Department of Physics, IIT Hyderabad, Kandi, Telangana 502285, India

[28] California Institute of Technology, 1200 East California Blvd, MC 249-17, Pasadena, CA 91125, USA

[29] Institute of Theoretical Astrophysics, University of Oslo. P.O. Box 1029 Blindern, NO-0315 Oslo, Norway

[30] Instituto de Fisica Teorica UAM/CSIC, Universidad Autonoma de Madrid, 28049 Madrid, Spain

[31] Center for Astrophysical Surveys, National Center for Supercomputing Applications, 1205 West Clark St., Urbana, IL 61801, USA

[32] Department of Astronomy, University of Illinois at Urbana-Champaign, 1002 W. Green Street, Urbana, IL 61801, USA

[33] Santa Cruz Institute for Particle Physics, Santa Cruz, CA 95064, USA

[34] Center for Cosmology and Astro-Particle Physics, The Ohio State University, Columbus, OH 43210, USA

[35] Department of Physics, The Ohio State University, Columbus, OH 43210, USA

[36] Jet Propulsion Laboratory, California Institute of Technology, 4800 Oak Grove Dr., Pasadena, CA 91109, USA

[37] George P. and Cynthia Woods Mitchell Institute for Fundamental Physics and Astronomy, and Department of Physics and Astronomy, Texas A&M University, College Station, TX 77843, USA

[38] LPSC Grenoble - 53, Avenue des Martyrs 38026 Grenoble, France

[39] Institució Catalana de Recerca i Estudis Avançats, E-08010 Barcelona, Spain

[40] Department of Physics, Carnegie Mellon University, Pittsburgh, Pennsylvania 15312, USA

[41] Observatório Nacional, Rua Gal. José Cristino 77, Rio de Janeiro, RJ - 20921-400, Brazil

[42] Department of Physics and Astronomy, Pevensey Building, University of Sussex, Brighton, BN1 9QH, UK

[43] Department of Physics, Northeastern University, Boston, MA 02115, USA

[44] Centro de Investigaciones Energéticas, Medioambientales y Tecnológicas (CIEMAT), Madrid, Spain

[45] Computer Science and Mathematics Division, Oak Ridge National Laboratory, Oak Ridge, TN 37831

[46]

[47] Cerro Tololo Inter-American Observatory, NSF's National Optical-Infrared Astronomy Research Laboratory, Casilla 603, La Serena, Chile

[48] Department of Astronomy, University of California, Berkeley, 501 Campbell Hall, Berkeley, CA 94720, USA

[49] Lawrence Berkeley National Laboratory, 1 Cyclotron Road, Berkeley, CA 94720, USA

This paper has been typeset from a TEX/LATEX file prepared by the author.